CrystEngComm

ARTICLE

Crystal engineering urea organic acid hydrogen bonded networks with solvent inclusion properties

Received 00th January 20xx,
Accepted 00th January 20xx

DOI: 10.1039/x0xx00000x

www.rsc.org/

Lucy K. Saunders[a,b], Harriott Nowell[b], Paul R. Raithby[a], Chick C. Wilson[a*]

Nine hydrogen bonded networks of *N*-phenylurea and 5-nitroisophthalic acid, with solvent inclusion properties, have been engineered and their thermal stabilities studied. Solvent guests of methanol, ethanol, acetonitrile, acetone, THF, ethyl acetate and water have been included into the hydrogen bonded host networks in pockets and channels *via* interaction with a carboxylic acid group of the host. Two non-solvated *N*-phenylurea 5-nitroisophthalic acid complexes (**NS1** 2:1 and **NS2** 1:1) were also formed. Thermal studies of the inclusion materials revealed guest release and conversion to **NS1**, in all but one case, and conversion of one non-solvated form to the other (**NS2** to **NS1**). The carboxylic acid:amide hydrogen bond synthon $\boldsymbol{R_2^2(8)}$ was shown to be a robust synthon for network formation whilst guest molecules are suggested to have a role in templating the overall network geometry.

Introduction

In crystal engineering, intermolecular interactions are exploited in the design of materials with desired structure related properties. [1] Inclusion materials have solid-state structures consisting of host and guest components. They are often targeted in crystal engineering because of their potential applications in pharmaceutics, [2] chemical sensing, [3] in the separation of alkanes [4] and in the capture of volatile organic compounds (VOCs). [5] In these host-guest systems, intermolecular interactions play a crucial role in host formation and often guest inclusion. [6, 7] Guest inclusion may be in channels, an inclusion compound, or by encapsulation within pockets, an inclusion clathrate. [8, 9] Guest uptake may be reversible [10] but may lead to structural collapse of the host framework; in this case the material can be said to have virtual porosity only. [11, 12]

A number of inclusion materials have been reported based on hydrogen bonded networks [13-15] where particular hydrogen bonding synthons assemble to build up the host structure. [16-18] Commonly exploited interactions are N—H···O hydrogen bonds, facilitating hexagonal channel formation in urea inclusion compounds, and carboxylic acid $R_2^2(8)$ [19, 20] hydrogen bonded dimer synthons, responsible for the honeycomb structure of the inclusion clathrate of trimesic acid coronene. [21] Urea is a particularly favourable molecular building block in hydrogen bonded network design having the potential to interact with a number of different co-formers *via* its different functional groups. The urea amide functionality means that, with organics acids containing carboxylic acid groups, the carboxylic acid:amide $R_2^2(8)$ hydrogen bonding synthon may form. Alhalaweh *et al.* (2010) defined three hydrogen bonding motifs that may result from the formation of this synthon between ureas (U) and organic acids (A) including a U:A, U:A:U or A:U:A hydrogen bonded motif; which is formed may be determined by the molecular building block substitution and stoichiometry. [22] These motifs have led to hydrogen bonded chains in substituted ureas with di-carboxylic acids. [23, 24] Amine groups have also been reported to facilitate extended hydrogen bond network formation in combination with nitro group functionality such as

[a.] *Department of Chemistry, University of Bath, Bath, BA2 7AY, UK.*
[b.] *Diamond Light Source, Harwell Science and Innovation Campus, Didcot OX11 0DE, UK.*
[c.] *Email: C.C.Wilson@bath.ac.uk*

†Electronic Supplementary Information (ESI) available: CIFs for **IM1** to **IM7**, **CIM1**, **CIM2**, **NS1** and **NS2**; crystal structure refinement details; selected molecular geometry tables, selected hydrogen bond tables; TG-MS, DSC and PXRD data. CCDC 1471780-147190 See DOI: 10.1039/x0xx00000x

in co-crystals of 3,5-dinitrobenzoic acid and 4-aminobenzoic acid; the nitro groups link to an amine group in the next molecule *via* bifurcated $R_2^1(4)$ and $R_2^2(8)$ hydrogen bond synthons [19, 25].

In this work we present nine inclusion materials (**IMs**) formed between the urea derivative of *N*-phenylurea and the polycarboxylic acid of 5-nitroisophthalic acid in the presence of a range of solvent guests (Scheme 1). Seven of the inclusion materials have host networks based on hydrogen bonded rings whilst two have condensed hydrogen bonded networks (**CIMs**). Five of the inclusion hosts based on rings are structurally similar. A number of hydrogen bond synthons form to make up the host networks (Scheme 2); a carboxylic acid:amide $R_2^2(8)$ hydrogen bond synthon forms in all cases and interaction with the guest is *via* a carboxylic acid hydroxyl group which does not participate in host framework formation. Two non-solvated forms (**NS**) of the host were also crystallised and are reported.

Experimental

Evaporative crystallisation

The inclusion materials were formed via evaporative crystallisation of a 2:1 stoichiometric ratio of the *N*-phenylurea and 5-nitroisophthalic acid host components (1:1 for **CIM1**) from a minimum volume of solvent.

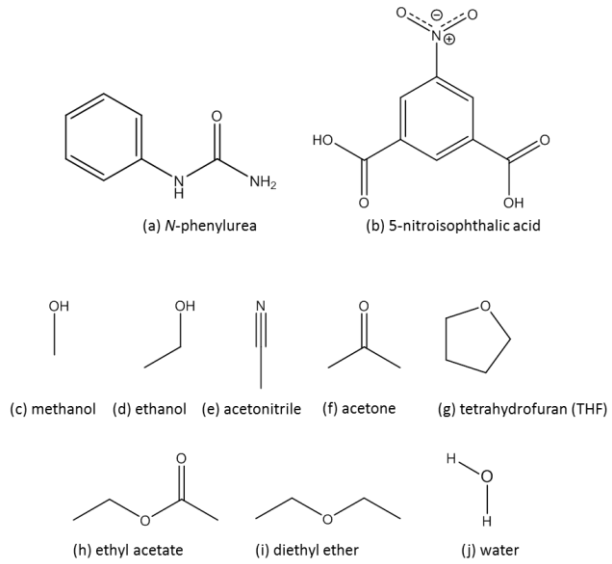

Scheme 1 – Components: (a) to (b) forming the host and (c) to (j) the solvent guests.

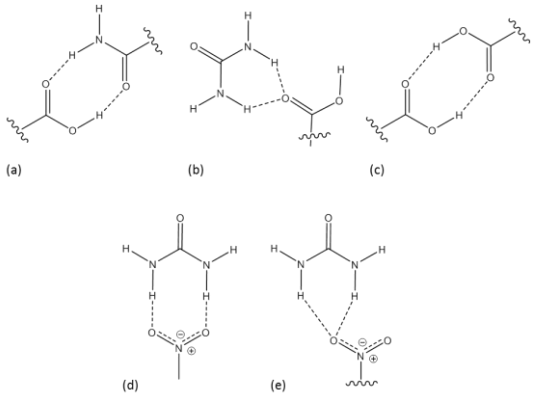

Scheme 2 – Hydrogen bond synthons: carboxylic acid:amide (a) $R_2^2(8)$ and (b) $R_2^1(6)$, (c) carboxylic acid dimer $R_2^2(8)$, nitro:amide (d) $R_2^2(8)$ and $R_2^1(6)$.

Inclusion material 1 (IM1) – Yellow block shaped crystals of the 7:4:2 complex of *N*-phenylurea, 5-nitroisophthalic acid and methanol were grown from methanol solvent at 40 °C.

Inclusion material 2 (IM2) – Yellow needle shaped crystals of the 3:2:1:1 complex of *N*-phenylurea, 5-nitroisophthalic acid, ethanol and water were grown from ethanol solvent at room temperature.

Inclusion material 3 (IM3) – Yellow block shaped crystals of the 3:2:1 complex of *N*-phenylurea, 5-nitroisophthalic acid and acetonitrile were grown from acetonitrile solvent at 40 °C.

Inclusion material 4 (IM4) – Yellow plate shaped crystals of the 3:2:1:1 complex of *N*-phenylurea, 5-nitroisophthalic acid, acetone and water were grown from acetone solvent at 30 °C.

Inclusion material 5 (IM5) – Yellow block shaped crystals of the 3:2:1:1 complex of *N*-phenylurea, 5-nitroisophthalic acid, THF and water were grown from THF solvent at 30 °C.

Inclusion material 6 (IM6) – Yellow plate shaped crystals of the 3:2:1 complex of *N*-phenylurea, 5-nitroisophthalic acid and ethyl acetate were grown from ethyl acetate solvent at room temperature.

Inclusion material 7 (IM7) – Yellow block shaped crystals of the 1:1:0.5:1 complex of *N*-phenylurea, 5-nitroisophthalic acid, THF and methanol were grown from a 50:50 solvent volume mix of THF and methanol solvent, at room temperature.

Condensed inclusion material 1 (CIM1) – Yellow fine needle shaped crystals of the 2:2:2 complex of *N*-phenylurea, 5-nitroisophthalic acid and water were grown from ethyl acetate solvent at room temperature.

Condensed inclusion material 2 (CIM2) – Colourless rectangular block shaped crystals of the 1:1:1 complex of *N*-phenylurea, 5-

nitroisophthalic acid and acetone were grown from acetone solvent at 4 °C.

Non-solvated form 1 (NS1) – Pale yellow plate shaped crystals of the 2:1 complex of *N*-phenylurea and 5-nitroisophthalic acid were grown from water at room temperature.

Non-solvated form 1 (NS2) – Yellow plate shaped crystals of the 1:1 complex of *N*-phenylurea and 5-nitroisophthalic acid were grown from diethyl ether at 30°C.

X-ray crystallography

Single crystal X-ray diffraction data were collected on **IM1**, **IM4** and **NS1** using a Rigaku Oxford Diffraction Xcalibur diffractometer equipped with an EosS2 detector using Mo-Kα radiation (λ = 0.71073 Å) and collected on **IM3**, **IM5**, **IM6**, **IM7**, **CIM1**, **CIM2** and **NS2** using a Rigaku Oxford Diffraction Supernova Dual Source diffractometer equipped with an EosS2 (**IM5**, **IM6**, **CIM1** and **CIM2**) or an Atlas (**IM3** and **IM7**) detector using Cu-Kα radiation (λ = 1.54184 Å). The sample temperature was controlled using Oxford Diffraction Cryostream apparatus (Cryostream and Cryostream plus) and the data processed using CrysAlisPro[26] version 1.171.37.33 (version 1.171.37.35 in the case of **CIM1)**. Single crystal X-ray diffraction data were collected on **IM2** at the Advanced Light Source (Berkeley, USA) using a Bruker AXS D8 diffractometer and PHOTON 100 CMOS detector with radiation 0.9538 Å. The sample temperature was controlled using an Oxford Cryosystems Cryostream Plus and the data processed using Bruker AXS APEX2 software. [27, 28] The structures were solved by direct methods using SHELXS-2013[29] and refinement was carried out in SHELXL-2013[30] within the WinGX package. [31] All non-hydrogen atoms were refined anisotropically except in the case of **IM2** and **IM7** where the solvent guests were disordered and so refined isotropically. Hydrogen atoms were treated by a mixture of independent and constrained refinements, located from Fourier difference maps or in calculated positions (Table S1†). Crystallographic data for all complexes are given in Table 1 and 2.

Thermogravimetric analysis coupled with mass spectrometry (TG-MS)

TG analysis was performed using a SETSYS Evolution TGA from Setaram Instrumentation, KEP Technologies. Samples (5 to 10 mg) were measured in an Alumina crucible, 170 µl, under an Argon gas purge, flow rate 20 ml min^{-1}. A heating regime of 5 °C min^{-1}, between 20 and 400 °C, was carried out on each sample, programmed using Calisto. MS was coupled with the TG analysis using an OmniStar GSC 320 from Pfeiffer Vacuum, under an Argon atmosphere (2.3 bar outlet pressure), programme using QUADERA. Mass loss data was determined using the Calisto software.

Differential scanning calorimetry (DSC)

DSC studies were carried out using a Thermal Advantage Q20 DSC from TA Instruments, equipped with Thermal Advantage Cooling System 90 and operated with a dry nitrogen purge gas at a flow rate of 18 cm^3 min^{-1}. Samples (3 to 6 mg) were each loaded in a Tzero™ aluminium pan sealed with a Tzero™ aluminium lid and a heating regime of 5 °C min^{-1}, between 20 and 290 °C, was carried out. Data were collected using the software Advantage for Qseries. Melting points and transition temperatures were derived using the TA Universal Analysis software.

Table 1 Crystallographic data for **IM1** to **IM6**.

Material	IM1	IM2	IM3	IM4	IM5	IM6
Formula	$C_{83}H_{84}N_{18}O_{33}$	$C_{39}H_{42}N_8O_{17}$	$C_{39}H_{37}N_9O_{15}$	$C_{40}H_{42}N_8O_{17}$	$C_{41}H_{44}N_8O_{17}$	$C_{41}H_{42}N_8O_{17}$
Molecular weight ($gmol^{-1}$)	1861.8	894.80	871.78	906.81	920.84	918.82
T (K)	150	100	150	150	150	150
Space group	P-1	P-1	P-1	P-1	P-1	P-1
a (Å)	12.2579(6)	6.9335(3)	10.0887(5)	12.3639(7)	12.3606(5)	9.8732(4)
b (Å)	14.7289(9)	12.4902(7)	12.3161(5)	13.0486(10)	13.4644(6)	10.9970(3)
c (Å)	23.5050(14)	25.4854(13)	17.3345(10)	13.8208(10)	14.3535(6)	20.4449(6)
α (°)	94.490(5)	89.062(5)	70.478(5)	71.686(7)	81.404(4)	80.035(2)
β (°)	91.215(4)	83.694(4)	87.122(4)	89.156(5)	83.684(4)	89.288(3)
γ (°)	90.291(4)	74.923(3)	87.659(4)	87.439(5)	64.194(4)	77.290(3)
Volume ($Å^3$)	4229.6(4)	2118.02(19)	2026.83(18)	2114.7(3)	2123.73(17)	2131.99(12)
Z	2	2	2	2	2	2
Reflections collected	37793	20333	14449	15520	15570	16547
Independent	16015	7477	7975	7468	8144	8157
Observed I>2σ	9340	3492	6311	2729	6568	6377
R_{int}	0.0423	0.0901	0.022	0.097	0.029	0.039
Parameters	1518	561	716	606	760	763
GooF	1.015	1.005	1.041	0.959	1.034	1.008
R_1 (observed)	0.0553	0.1019	0.0396	0.0834	0.0509	0.0539
R_1 (all)	0.1125	0.1972	0.0526	0.2373	0.0633	0.0687

wR_2 (all)	0.1460	0.3331	0.1125	0.2000	0.1470	0.1547

Table 2 Crystallographic data for **IM7, CIM1, CIM2** and the non-solvated forms **NS1** and **NS2**.

Material	**IM7**	**CIM1**	**CIM2**	**NS1**	**NS2**
Formula	$C_{18}H_{21}N_3O_{8.5}$	$C_{30}H_{30}N_6O_{16}$	$C_{18}H_{19}N_3O_8$	$C_{22}H_{21}N_5O_8$	$C_{15}H_{13}N_3O_7$
Molecular weight ($gmol^{-1}$)	415.38	730.6	405.36	483.44	347.28
T (K)	150	150	150	150	150
Space group	P-1	P-1	$P2_1/c$	P-1	$P2_1/c$
a (Å)	9.9483(8)	6.8562(5)	7.7787(1)	8.9131(7)	15.1254(3)
b (Å)	9.9564(8)	11.9649(9)	18.8747(2)	9.7105(8)	12.7462(2)
c (Å)	10.6641(7)	20.6362(10)	13.0343(1)	13.3778(11)	16.2905(4)
α (°)	66.488(7)	78.951(5)	90	71.440(7)	90
β (°)	75.790(7)	88.870(5)	91.528 (1)	78.479(7)	107.286(3)
γ (°)	71.335(7)	76.106(6)	90	83.019(7)	90
Volume ($Å^3$)	909.16(13)	1612.26(19)	1913.02(4)	1073.43(16)	2998.81(12)
Z	2	2	4	2	8
Reflections collected	6117	11673	12893	8876	20298
Independent	3565	6168	3711	4920	6023
Observed I>2σ	3029	5069	3376	3277	4827
R_{int}	0.0141	0.0291	0.0272	0.026	0.031
Parameters	274	483	338	400	555
GooF	1.081	1.087	1.029	1.0230	1.123
R_1 (observed)	0.0642	0.0848	0.0345	0.0520	0.0526
R_1 (all)	0.0721	0.0975	0.0376	0.0930	0.0659
wR_2 (all)	0.2040	0.2446	0.0969	0.1101	0.1426

Hot stage microscopy (HSM)

HSM was carried out using a Mettler Toledo FP82 hot stage equipped with a Leica DM1000 microscope. Each sample was placed in the sample chamber and subjected to a programmed temperature regime using the FP90 Central Processor. Samples were filmed using an Infinity 2 microscopy camera. Single crystals of each complex were heated from ambient temperature to a final temperature of 290 °C, at a rate of 5 °C per minute. Powder samples of each complex were heated from ambient temperature to just above the transition temperatures (145 or 150 °C and 184 or 189 °C), at a rate of 5 °C per minute.

Powder X-ray diffraction (PXRD)

PXRD data were collected in flat plate mode on a Bruker D8 Advance equipped with monochromated Cu-Kα radiation (λ=1.54056 Å) in reflection geometry at 298 K. PXRD patterns were collected on powder samples at room temperature and after heating on the HSM to just above the transition temperatures. Data were collected in the *2Θ* range 5-50 °.

Results and Discussion

Inclusion materials synthesis

Nine solvent inclusion materials (**IM1 – IM7**, **CIM1** and **CIM2**) and two non-solvated networks (**NS1**) and (**NS2**) were synthesised from the *N*-phenylurea and 5-nitroisophthalic acid host components in the presence of a range of solvents by evaporative crystallisation. The host components were set up in three different ratios of 1:1, 2:1 and 1:2 with the different solvents; it was thought that on changing the stoichiometry, different hydrogen bonding networks might result as the number of different groups available for each type of synthon formation is changed. In particular, the formation of the carboxylic acid:amide $\boldsymbol{R_2^2(8)}$ hydrogen bond synthon was likely to be affected by the set up ratio of the *N*-phenylurea (U) and 5-nitroisophthalic acid (A) components; a 1:1 set up ratio would favour the formation of this synthon involving one 5-nitroisophthalic acid carboxylic acid group (in a U:A motif) whilst a 2:1 ratio would favour its formation involving both carboxylic acid groups (in a U:A:U motif). [22] In fact, changing the set up ratio of components did not appear to change the host network; the same network was favoured for each solvent regardless of stoichiometric ratio of components. Changes in the host network were instead achieved on changes to the guest; a different structure was observed for when acetone or water were included on their own compared to when included together.

Not all the solvents trialled generated inclusion materials; the host components were set up in a range of polar (methanol, ethanol, acetonitrile, acetone, THF, ethyl acetate, water) and non-polar solvents (diethyl ether, hexane and cyclohexane) singly and in 50:50 mixtures. Only the polar solvents formed inclusion materials; diethyl ether produced **NS2** whilst the host components were insoluble in hexane and cyclohexane. Water was frequently included in the host network alongside the crystallisation solvent (**IM2**, **IM4**, **IM5**). In most cases, with the exception of **IM7**, the 50:50 mixtures led to the inclusion of one of the solvents only.

Host crystal structures

In inclusion materials **IM1** – **IM7**, *N*-phenylurea and 5-nitroisophthalic acid molecules assemble into hydrogen bonded ring host networks around solvent guest molecules (Fig. 1 (a) to (g)). The hydrogen bonded ring network is comprised of eight molecular building blocks in **IM1** – **IM6** and in each case molecular assembly is *via* four carboxylic acid:amide $\boldsymbol{R_2^2}(8)$ hydrogen bond synthons, in both U:A and U:A:U hydrogen bonded motifs, and *via* two carboxylic acid:amide $\boldsymbol{R_2^1}(6)$ and two nitro:amide $\boldsymbol{R_2^2}(8)$ hydrogen bond synthons (Table 3 and Table 4). In contrast, six molecular building blocks form the hydrogen bonded ring in **IM7** and molecular assembly occurs *via* two carboxylic acid:amide $\boldsymbol{R_2^2}(8)$ hydrogen bond synthons, in a U:A motif, and *via* two nitro:amide $\boldsymbol{R_2^1}(6)$ hydrogen bond synthons and two carboxylic acid dimer $\boldsymbol{R_2^2}(8)$ hydrogen bond synthons.

Condensed hydrogen bonded networks form in **CIM1** and **CIM2** (Fig. 1 (h) and (i)), each containing different portions of the ring networks present in **IM1 – IM6**; carboxylic acid:amide $R_2^2(8)$ hydrogen bond synthons, in a U:A motif, form in both alongside a nitro:amide $R_2^2(8)$ hydrogen bond synthon in **CIM1** and a carboxylic acid:amide $R_2^1(6)$ synthon in **CIM2**. Ring formation does not occur in **CIM1** and **CIM2** for the 1:1 stoichiometry of the host components; only one U:A motif is possible for this stoichiometry, involving one 5-nitroisophthalic acid carboxylic acid group, whilst the second interacts with the solvent guest. In each hydrogen bonded network, there are structural variations in the molecular building blocks (Table S2†). These are most significant for *N*-phenylurea occurring in the angles between the urea and phenyl moiety planes; variation occurs across the IMs and within the same crystal structure. In general, the co-planarity of the phenyl and urea moieties is increased in the IMs compared to the native crystal structure; angles between the plane of the two moieties range from ca. 0 to 35 ° in the IMs versus ca. 48 ° in the native crystal structure CSD Refcode PHUREA01. [32]

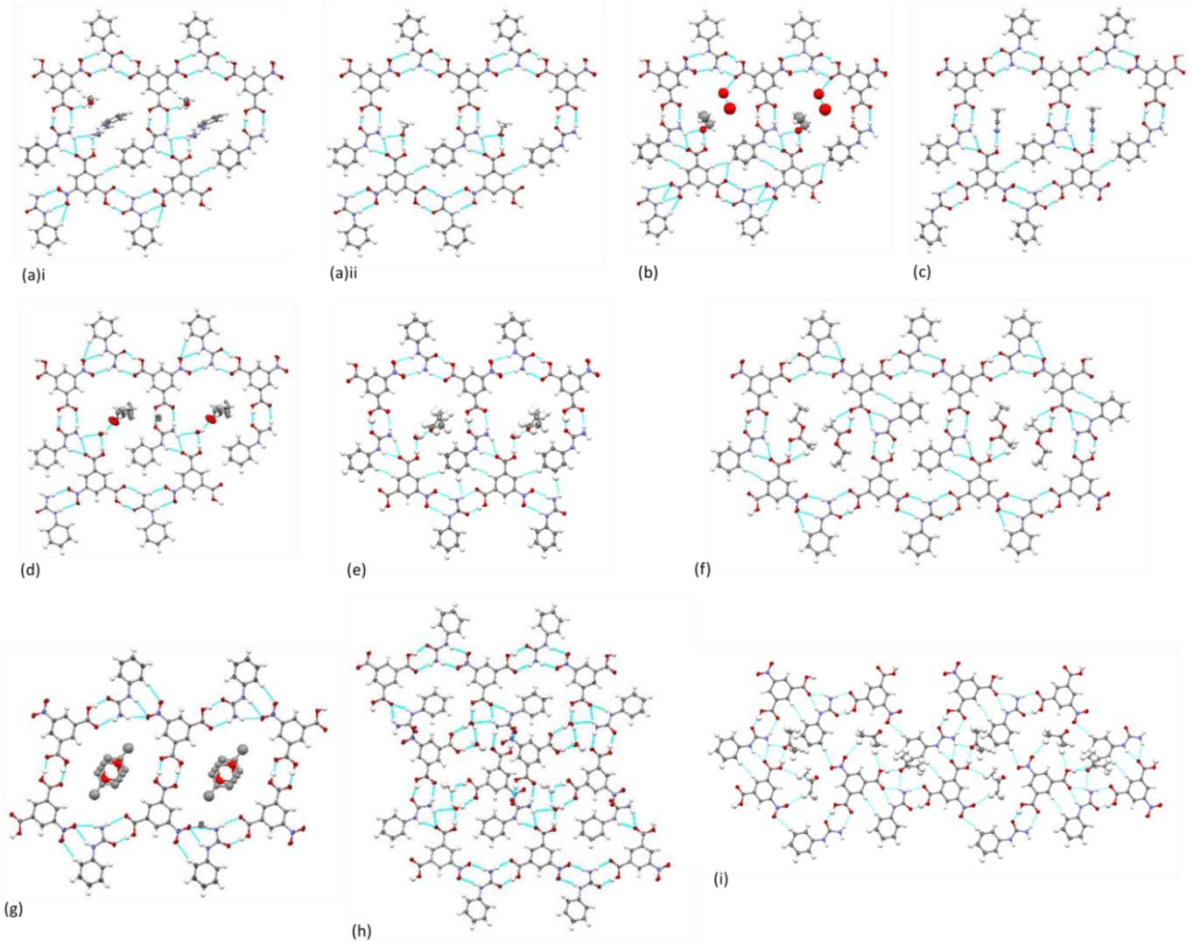

Fig. 1 Hydrogen bonded networks in one layer of the *N*-phenylurea 5-nitroisophthalic inclusion materials (a) i and ii (two types of guest inclusion) **IM1**, (b) **IM2**, (c) **IM3**, (d) **IM4**, (e) **IM5**, (f) **IM6**, (g) **IM7**, (h) **CIM1** and (i) **CIM2**.

Table 3 Hydrogen bond donor acceptor distances (D···A) in the hydrogen bond networks of **IM1** to **IM6**, **CIM1** and **CIM2**. See Table S3† to S6† for the full details of the hydrogen bonding.

IM	Carboxylic acid:amide synthon $R_2^2(8)$		Carboxylic acid:amide synthon $R_2^1(6)$		Nitro:amide synthon $R_2^2(8)$	
	D-H...A	d(D...A) (Å)	D-H...A	d(D...A) (Å)	D-H...A	d(D...A) (Å)
IM1	N(14)-H(26)...O(8)	3.044(3)	N(13)-H(28)...O(20)	2.899(3)	N(3)-H(41)...O(29)	3.064(3)
	O(7)-H(102)...O(14)	2.500(2)	N(14)-H(27)...O(20)	3.085(3)	N(4)-H(56)...O(30)	3.157(3)
	N(3)-H(42)...O(32)	2.877(3)	N(2)-H(53)...O(28)	2.927(3)	N(6)-H(16)...O(10)	3.273(3)
	O(31)-H(79)...O(26)	2.632(2)	N(1)-H(52)...O(28)	3.042(3)	N(7)-H(17)...O(9)	2.980(3)
	N(1)-H(51)...O(5)	2.984(3)			N(9)-H(72)...O(1)	3.006(3)
	O(6)-H(80)...O(25)	2.520(3)			N(8)-H(74)...O(2)	3.265(3)
	N(9)-H(73)...O(4)	2.882(3)			N(11)-H(14)...O(16)	2.986(3)
	O(3)-H(81)...O(21)	2.555(2)			N(10)-H(12)...O(15)	3.179(3)
	N(11)-H(77)...O(18)	2.850(3)				
	O(17)-H(83)...O(13)	2.595(2)				
	N(7)-H(101)...O(11)	2.902(3)				
	O(12)-H(82)...O(23)	2.559(2)				
IM2	O(1)-H(3)...O(14)	2.534(6)	N(4)-H(12)...O(7)	3.150(7)	N(5)-H(19)...O(3)	3.384(7)
	N(6)-H(20)...O(2)	2.961(7)	N(3)-H(13)...O(7)	2.923(7)	N(6)-H(21)...O(4)	3.043(7)
	O(6)-H(1)...O(13)	2.514(6)			N(7)-H(29)...O(11)	3.371(7)
	N(4)-H(11)...O(5)	3.061(7)			N(8)-H(28)...O(12)	3.020(7)
	O(10)-H(6)...O(15)	2.580(6)				
	N(8)-H(27)...O(9)	2.904(6)				
IM3	O(6)-H(21)...O(1)	2.5566(15)	N(1)-H(6)...O(2)	3.0254(16)	N(6)-H(13)...O(14)	2.9580(18)
	N(3)-H(14)...O(10)	2.8559(17)	N(7)-H(5)...O(2)	2.9087(17)	N(5)-H(27)...O(12)	3.2791(17)
	O(3)-H(20)...O(4)	2.5256(15)			N(2)-H(16)...O(13)	3.2152(17)
	N(7)-H(4)...O(9)	2.9706(17)			N(3)-H(15)...O(15)	2.9873(18)
	O(8)-H(23)...O(5)	2.5538(15)				
	N(6)-H(12)...O(11)	2.8939(19)				
IM4	O(7)-H(42)...O(5)	2.572(5)	N(7)-H(52)...O(13)	2.914(6)	N(3)-H(3B)...O(9)	3.038(6)
	N(4)-H(4A)...O(10)	2.862(6)	N(10)-H(10B)...O(13)	3.113(6)	N(2)-H(51)...O(6)	3.280(6)
	O(1)-H(1)...O(4)	2.506(6)			N(4)-H(4B)...O(8)	3.021(6)
	N(10)-H(10A)...O(12)	2.966(7)			N(6)-H(50)...O(15)	3.236(7)
	O(3)-H(60)...O(11)	2.576(5)				
	N(3)-H(3A)...O(14)	2.894(5)				
IM5	O(4)-H(43)...O(13)	2.5333(19)	N(7)-H(38)...O(11)	3.153(2)	N(4)-H(6)...O(1)	3.363(2)
	N(7)-H(39)...O(3)	3.022(2)	N(8)-H(37)...O(11)	2.942(2)	N(3)-H(7)...O(2)	2.964(2)
	O(6)-H(41)...O(15)	2.5115(19)			N(5)-H(15)...O(8)	3.034(2)
	N(3)-H(8)...O(5)	2.918(2)			N(6)-H(16)...O(9)	3.270(2)
	O(7)-H(4)...O(14)	2.6112(19)				
	N(5)-H(14)...O(10)	2.900(2)				
IM6	O(4)-H(33)...O(8)	2.5288(19)	N(7)-H(29)...O(15)	2.928(2)	N(6)-H(21)...O(1)	3.342(2)
	N(8)-H(13)...O(3)	2.927(2)	N(8)-H(14)...O(15)	2.927(2)	N(5)-H(19)...O(2)	3.001(2)
	O(5)-H(42)...O(7)	2.525(2)			N(4)-H(1)...O(6)	2.929(2)
	N(4)-H(1)...O(6)	2.929(2)			N(3)-H(3)...O(12)	3.257(2)
	O(9)-H(20)...O(11)	2.574(2)				
	N(5)-H(18)...O(10)	2.871(2)				
CIM1	O(13)-H(13)...O(1)	2.516(4)	N(4)-H(4A)...O(3)	2.955(4)	N(2)-H(2A)...O(6)	3.137(4)
	N(5)-H(5A)...O(12)	2.954(4)	N(5)-H(5B)...O(3)	2.977(4)	N(3)-H(3B)...O(7)	2.962(4)
CIM2	O(1)-H(3)...O(7)	2.5057(11)	N(3)-H(8)...O(3)	3.0673(13)		
	N(3)-H(9)...O(2)	2.9600(13)	N(2)-H(7)...O(3)	2.9058(12)		

Table 4 Hydrogen bond donor acceptor distances in the hydrogen bond networks of **IM7**. See Table S3† to S6† for the full details of the hydrogen bonding.

	Carboxylic acid:amide synthon $R_2^2(8)$		Carboxylic acid dimer synthon $R_2^2(8)$		Nitro:amide synthon $R_2^1(8)$	
	D-H...A	d(D...A) (Å)	D-H...A	d(D...A) (Å)	D-H...A	d(D...A) (Å)
IM7	O(2)-H(5)...O(7)	2.534(2)	O(6)-H(1)...O(5)	2.623(2)	N(3)-H(6)...O(4)	3.045(3)
	N(3)-H(7)...O(1)	3.007(3)			N(2)-H(8)...O(4)	3.143(2)

The variation in the torsion angles of the 5-nitroisophthalic acid carboxylic acid groups with the benzene ring across the IMs is only small in comparison (OCCC torsions in the range of 0 to 12 °). There does not appear to be any link between hydrogen bond synthon involvement and the structural variations.

At first glance, the host ring networks in **IM1** – **IM5** appear isostructural, having the same graphset notation $\boldsymbol{R_8^8}(42)$. However, the arrangement of the hydrogen bond synthons in space, and the orientation of the molecular building blocks differs (Fig. 2). The hydrogen bonded network in **IM6** contains the same number of each hydrogen bond synthon as in **IM1** – **IM5** but has an expanded ring structure with a different graphset notation of $\boldsymbol{R_8^8}(40)$. In **IM7**, a different combination of synthons to **IM1** – **IM6**, are present and the overall hydrogen bonding network is altered, with graphset notation $\boldsymbol{R_6^6}(36)$.

The longest dimension of the hydrogen bonded ring in each inclusion material is approximately 12 Å in **IM1** – **IM5** and 15 Å in **IM6** and **IM7**, where the network is expanded.

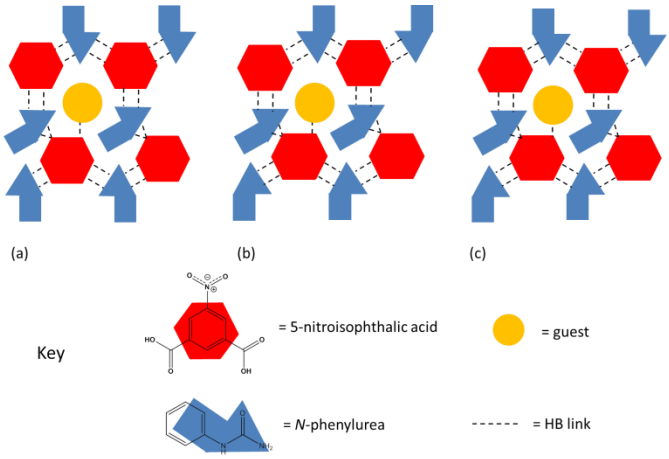

Fig. 2 The different orientations of the *N*-phenylurea molecular building blocks in structurally similar (a) **IM1**, **IM2** and **IM4,** (b) **IM3** and (c) **IM5**.

These dimensions are comparable to those for the inclusion materials of trimesic acid (14 Å), if there is no pore interpenetration, [33] 2,4,6-tris-(4-bromophenoxy)-1,3,5-triazine (BrPOT) (12 Å) [34] and in some zeolites. [35]

Guest inclusion

Guests (G) are included in the centre of the hydrogen bonded ring in each IM and in the close packed space in the CIMs. The host:guest ratios are presented in Table 5. In **IM1**, **IM3**, **IM6**, **CIM1** and **CIM2**, a single type of guest species is included in the host structure. In contrast, in **IM4**, **IM5** and **IM7**, two types of guest species are included; in **IM4** and **IM5** a volatile solvent and a water molecule are included whilst in **IM7** a disordered THF and methanol molecule are included. Guest inclusion occurs in **IM1** – **IM6** and **CIM1** and **CIM2** by tethering to a carboxylic acid hydroxyl group of the host *via* an O—H···O or O—H···N hydrogen bond that is not involved in formation of the hydrogen bonded host

Table 5 Host-guest ratios in the complexes studied, per asymmetric unit.

IM	No. of *N*-phenylurea molecules	No. of 5-nitroisophthalic acid molecules	No. of guest molecules
IM1	7	4	2
IM2	3	2	2
IM3	3	2	1
IM4	3	2	2
IM5	3	2	2
IM6	3	2	1
IM7	1	1	1.5
CIM1	1	1	1
CIM2	1	1	1

network; the hydroxyl group interacts with an oxygen or nitrogen atom on the solvent guest. In contrast, in **IM7**, the hydrogen bonding capacity of the host building blocks is satisfied in network formation and there is no carboxylic acid hydroxyl group to which the guest can tether. Instead, the guest species are held in place by π-interactions to host rings in the layers above and below ($d_{\pi\cdots\pi}$ 3.220(5) to 3.316(5) Å). The host-guest and guest-guest interaction distances in all the IMs and CIMs are presented in Table 6. In **IM1**, two types of guest inclusion occurs (Fig. 1(a) i and ii). In one host ring, a methanol guest is tethered to the host by interaction to the carboxylic acid hydroxyl group. In the second host ring, a molecule of *N*-phenylurea hydrogen bonds instead to the carboxylic acid hydroxyl group, through an O—H···O hydrogen bond, and the methanol guest interacts with the host through a side on O—H···O hydrogen bond to a carbonyl oxygen in an carboxylic acid:amide synthon. In **IM4** and **IM5**, water acts as the tether to the host framework by interacting with the carboxylic acid hydroxyl group and the second solvent molecule is held in place by a guest-guest

Table 6 Host-guest (H-G), guest-guest (G-G) interaction distances (D···A) in the IMs. See Table S7† for the full details of the hydrogen bonding.

IM	Interaction type	D-H...A	d(D...A) (Å)
IM1	H-G (host-methanol1)	O(27)-H(78)...O(100)	2.603(3)
	H-G (host-methanol1)	O(100)-H(106)...O(26)	2.801(3)
	H-G (host-methanol2)	O(101)-H(107)...O(8)	2.783(3)
	H-G (host-methanol2)	N(16)-H(48)...O(101)	2.918(3)
	H-G (host-N-phenylurea)	O(19)-H(100)...O(22)	2.561(3)
IM2	H-G (host-ethanol)	O(8)-H(10)...O(16)	2.611(9)
	G-G (ethanol-water1)	O(16)...O(17)	2.75(2)
	G-G (water1-water2)	O(17)...O(18)	2.17(2)
IM3	H-G (host-acetonitrile)	O(7)-H(22)...N(9)	2.762(2)
IM4	H-G (host-water)	O(2)-H(2)...O(17)	2.626(7)
	H-G (host-water)	O(17)-H(53)...O(10)	2.859(8)
	G-G (water-acetone)	O(17)-H(54)...O(100)	2.795(10)
IM5	H-G (host-water)	O(12)-H(5)...O(17)	2.594(2)
	H-G (host-water)	O(17)-H(22)...O(14)	2.867(2)
	G-G (water-THF)	O(17)-H(23)...O(16)	2.805(3)
IM6	H-G (host-ethyl acetate)	O(14)-H(32)...O(16)	2.630(2)
IM7	H-G (host-THF/methanol)	π···π	3.220(5) – 3.316(8)
CIM1	H-G (host-water1)	O(2)-H(2B)...O(16)	2.555(4)
	H-G (host-water1)	O(16)-H(100)...O(10)	2.783(4)
	H-G (host-water2)	O(11)-H(105)...O(15)	2.690(4)
	H-G (host-water2)	O(15)-H(103)...O(8)	2.840(4)
	H-G (host-water2)	O(15)-H(102)...O(14)	2.691(4)
	G-G (water1-water2)	O(16)-H(101)...O(15)	2.778(5)
CIM2	H-G (host-acetone)	O(4)-H(1)...O(8)	2.6433(12)
	H-G (host-acetone)	N(3)-H(8)...O(8)	3.0691(13)

O—H···O hydrogen bond to the water. Additional interactions hold the water guest species in place in **CIM1**; one water hydrogen bonds to a second carboxylic acid group, this time to the carbonyl oxygen, whilst the other water molecule is held in place by an additional interaction to a nitro group and a urea carbonyl in neighbouring 5-nitroisophthalic acid and *N*-phenylurea molecules, respectively. Guest-guest interactions also occur between the two water molecules.

The hydrogen bonded rings in **IM1** – **IM7** pack in layers. In **IM1**, **IM3**, **IM4** and **IM5**, pairs of rings stack on top of one another in opposite orientations creating pockets of guests; this arrangement is characteristic of inclusion clathrates (Fig. 3). In **IM2**, **IM6** and **IM7**, hydrogen bonded rings stack continuously on top of one another, creating channels; this is characteristic of inclusion compounds (Fig. 4).

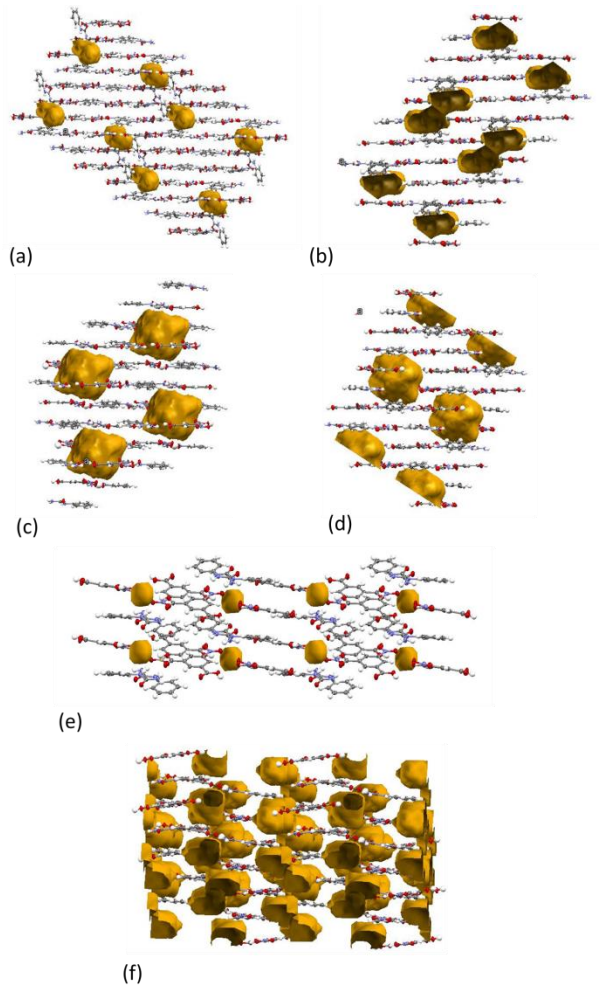

Fig. 3 Pockets occupied by the guest molecules in the *N*-phenylurea and 5-nitroisophthalic acid host framework in (a) **IM1**, (b) **IM3**, (c) **IM4**, (d) **IM5**, (e) **CIM1** and (f) **CIM2**.

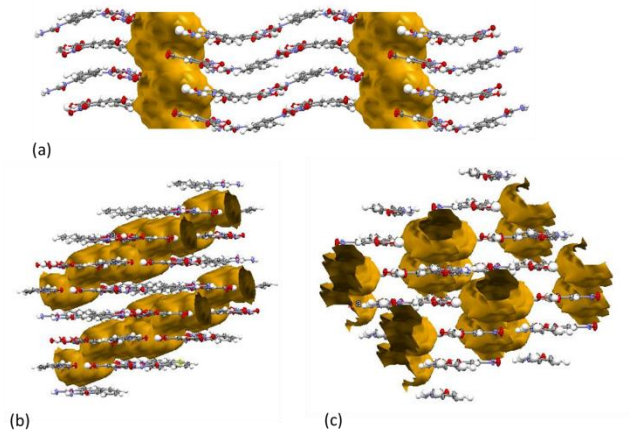

Fig. 4 Channels occupied by the guest molecules in the *N*-phenylurea and 5-nitroisophthalic acid host framework in (a) **IM2**, (b) **IM6** and (c) **IM7**.

In **IM2**, the layers are not planar but have a wave like structure and, in the case of **IM6** and **IM7**, the hydrogen bonded rings are stacked offset from one another and the guest channels run diagonally through the structure. There is some layering in the structures of **CIM1** and **CIM2** and the guests occupy pockets, in pairs (Fig. 3). The void spaces of the pockets and channels occupied by the guest molecules in **IM1** – **IM7**, **CIM1** and **CIM2** were mapped in Mercury [36] on a structural model with the solvent molecule(s) removed; the void spaces are shown in Fig. 3 and Fig. 4 in yellow. The void calculation in Mercury [36] used a contact surface with parameters of a 1.2 Å probe radius and 0.7 Å grid spacing (Table 7). Small void volumes were indicated in **CIM1** (< 14 Å^3 per unit cell), whilst the largest void volume was present in **CIM2** (~336 Å^3 per unit cell). **CIM2** was also shown to be the least dense 'empty framework' whilst **IM1** was the most dense.

Table 7 Calculated void volumes and densities in **IM1** – **IM7**, **CIM1** and **CIM2**.

IM	Unit cell volume occupied by void (%)	Void volume per unit cell (Å^3)	Calculated density with solvent removed (gmol^{-1}Å^{-3})
IM1	3.2	136.34	1.4368
IM2	12.8	270.32	1.3026
IM3	5.9	119.51	1.3612
IM4	11.5	243.00	1.3046
IM5	13.1	279.23	1.2991
IM6	12.6	268.28	1.2941
IM7	19.7	178.80	1.2309
CIM1	0.9	13.73	1.4308
CIM2	17.6	336.24	1.2058

Non solvated (NS) materials

Two non-solvated forms of *N*-phenylurea 5-nitrosiophthalic acid were also crystallised, **NS1**, in a 2:1 ratio of components, and **NS2**, in a 2:2 ratio (Fig. 5). **NS1** has a structurally similar hydrogen bonded ring network to that formed in **IM1** – **IM5**, comprised of four carboxylic acid:amide $\boldsymbol{R_2^2}(8)$ hydrogen bond synthons, in both U:A and U:A:U hydrogen bonded motifs, two carboxylic acid:amide $\boldsymbol{R_2^1}(6)$ and two nitro:amide $\boldsymbol{R_2^2}(8)$ hydrogen bond synthons. In contrast to **IM1** – **IM5**, in **NS1,** an *N*-phenylurea molecule sits in place of the guest in the centre of the ring and an additional carboxylic acid:amide $\boldsymbol{R_2^2}(8)$ hydrogen bond synthon is formed. **NS2** has a very different structure to all other complexes discussed here. A single carboxylic acid:amide $\boldsymbol{R_2^2}(8)$ hydrogen bond synthon is formed, in a U:A motif, alongside a nitro:amide $\boldsymbol{R_2^1}(6)$ hydrogen bond synthon and a single O—H···O interaction, formed between different 5-nitroisophthalic acid molecules and involving a carboxylic acid hydroxyl group of one and a carbonyl oxygen atom, participating in a carboxylic acid:amide $\boldsymbol{R_2^2}(8)$ synthon, in another. The hydrogen bonding interactions in **NS1** and **NS2** are listed in Table 7 and Table 8. Packing of the hydrogen bonded networks in **NS1** and **NS2** occurs in layers (Fig. 6).

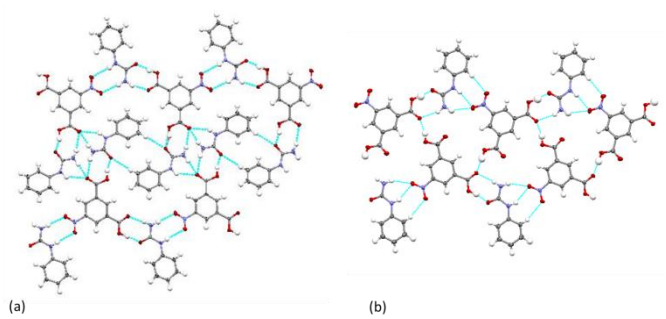

Fig. 5 Hydrogen bonded ring networks in *N*-phenylurea 5-nitroisophthalic non-solvated forms (a) **NS1** and (b) **NS2**.

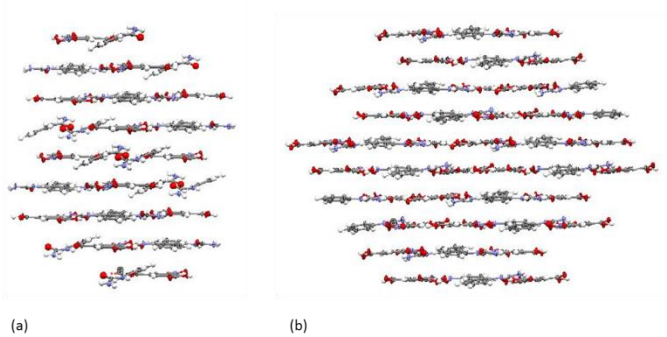

Fig. 6 Layered structures of *N*-phenylurea and 5-nitroisophthalic acid in non-solvated complexes (a) **NS1** and (b) **NS2**.

The *N*-phenylurea molecule occupying the centre of the hydrogen bonded ring in **NS1** is twisted relative to the hydrogen bonded ring network and packs diagonally across the ring layers.

Thermal behaviour

TG-MS, DSC and HSM were carried out on **IM1** – **IM7**, **CIM1** and **CIM2** to determine the thermal stability of these materials. The TG curves are shown in Fig. 7. The TG analysis shows well defined three-step mass loss profiles in each of the IM and CIM curves. The first step corresponds to the loss of the guest, with the identity of each lost guest confirmed by MS analysis (Fig. S9 † to Fig. S11 †). The second and third mass loss steps correspond to the *N*-phenylurea and 5-nitroisophthalic acid components, respectively, of the host framework. There was reasonable agreement between the expected and observed weight loss values for each step (Table S12†). The DSC traces for each IM and the non-solvated materials, **NS1** and **NS2**, are shown in Fig. 8 and the thermal data is tabulated in Table 9.

Table 7 Hydrogen bond donor acceptor distances (D···A) in the hydrogen bond networks of **NS1**. See Table S8† for the full details of the hydrogen bonding.

	Carboxylic acid:amide synthon $R_2^2(8)$		Carboxylic acid:amide synthon $R_2^1(6)$		Nitro:amide synthon $R_2^2(8)$	
	D-H...A	d(D...A) (Å)	D-H...A	d(D...A) (Å)	D-H...A	d(D...A) (Å)
NS1	O(6)-H(21)...O(1)	2.610(2)	N(4)-H(11)...O(3)	3.045(2)	N(2)-H(15)...O(7)	3.151(2)
	N(3)-H(14)...O(5)	2.889(3)	N(5)-H(10)...O(3)	3.113(2)	N(3)-H(13)...O(8)	3.084(3)
	O(4)-H(1)...O(2)	2.5232(18)				
	N(4)-H(12)...O(3)	3.135(2)				

Table 8 Hydrogen bond donor acceptor distances (D···A) in the hydrogen bond networks of **NS2.** See Table S8† for the full details of the hydrogen bonding.

	Carboxylic acid:amide synthon $R_2^2(8)$		Nitro:amide synthon $R_2^1(8)$		O—H···O Single HB	
	D-H...A	d(D...A) (Å)	D-H...A	d(D...A) (Å)	D-H...A	d(D...A) (Å)
NS2	O(8)-H(24)...O(1)	2.479(2)	N(1)-H(16)...O(12)	3.127(3)	O(6)-H(23)...O(14)	2.655(2)
	N(4)-H(21)...O(7)	3.068(3)	N(2)-H(14)...O(12)	3.121(3)	O(10)-H(1)...O(7)	2.661(2)
	O(13)-H(100)...O(2)	2.481(2)	N(3)-H(17)...O(4)	3.082(3)		
	N(2)-H(15)...O(14)	3.010(3)	N(4)-H(22)...O(4)	3.157(3)		

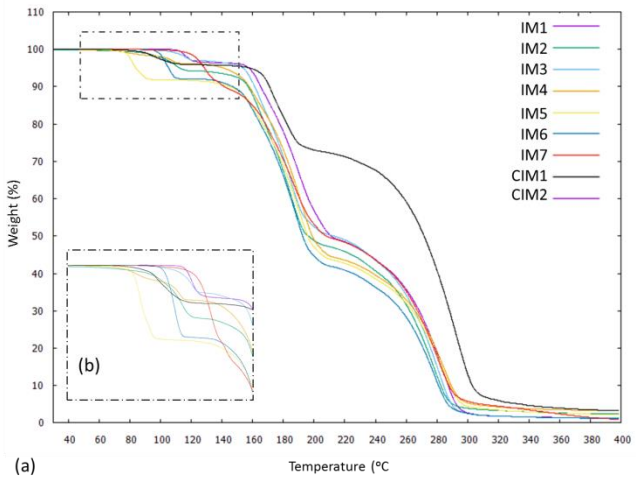

Fig. 7 TG curves of **IM1** – **IM7**, **CIM1** and **CIM2**: (a) over the full temperature range and (b) over desolvation range, at 5 °C min^{-1} heating rate.

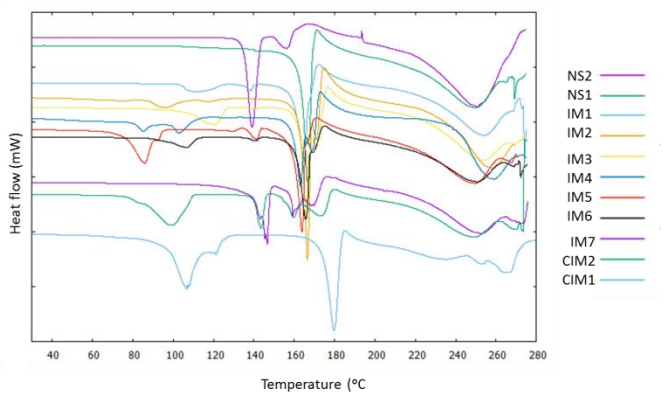

Fig. 8 DSC traces of **IM1** – **IM7**, **CIM1**, **CIM2**, **NS1** and **NS2**, recorded at a 5 °C min^{-1} heating rate.

The broad endotherms, below 130 °C, in the DSC trace for each IM correspond to the loss of the solvent guest from the host; these occur within the temperature range of the first mass loss step in the TG curves of each IM. Two endotherms are present in the case of **IM2**, **IM4** and **IM5**, where two types of guests occupy the host structure. The differing onset temperatures of the desolvation endotherms indicate there is a significant difference in energy required to remove each guest molecule from the host structure across the different IMs (Table S13†). Guest removal energy has previously been related to crystal density, where a more dense inclusion material is the most stable. [37] However, in this case, the energy required to remove each guest correlates more strongly with guest boiling point.

HSM on single crystals of **IM1** – **IM7**, **CIM1** and **CIM2** indicated loss of single crystallinity upon desolvation; a powder product was formed in each case. A melt present in the DSC traces of **IM1** – **IM7** and **CIM2**, post desolvation at T_{onset} ca. 150 °C, matches the main melt of **NS1**, suggesting the identity of the desolvation product as **NS1**. The short melt in the DSC trace of **NS2**, at T_{onset} 149.6 °C, also matches the main melt of **NS1**, suggesting conversion to **NS1** at this temperature. The recrystallisation peak in the DSC traces of **IM1** – **IM7**, **CIM2**, **NS1** and **NS2** at ca. T_{onset} 170 °C suggest conversion to the same unidentified product (**UN1**) at this temperature. Different thermal behaviour, post desolvation, is observed for **CIM1**. The main melt in the DSC trace occurs at a higher temperature of T_{onset} 174.2 °C followed by a recrystallisation at T_{onset} 185.7 °C; **CIM1** is not suggested to convert to **NS1** on desolvation but to a different unidentified product (**UN2**) which then converts to a further different unidentified product (**UN3**) post recrystallisation. The thermal transitions indicated in the DSC traces for each material were investigated by PXRD on powder samples at room temperature and after preheating on the hot-stage to the transition temperature.

Table 9 Thermal data of **IM1** – **IM7**, **CIM1**, **CIM2**, **NS1** and **NS2** from the DSC analysis.

Material	Endotherm 1 (°C)	Endotherm 2 (°C)	Melt 1 (°C)	Melt 2 (°C)	Melt 3 (°C)	Recrystallisation 1 (°C)
IM1	103.3		138.6	159.7		169.2
IM2	86.9	112.8		163.4	169.0	172.2
IM3	106.6		138.1	162.7	168.8	174.1
IM4	80.8	99.8		159.1	166.1	170.7
IM5	76.0	89.5	136.1	159.8	165.7	167.8
IM6	95.8		136.6	161.2	168.2	170.1
IM7	143.4			158.6	167.0	172.3
CIM1	96.6				174.2	185.7
CIM2	83.2		140.1	155.5	164.9	177.8
NS1				163.0		169.4
NS2			134.8	149.6		157.1

PXRD analysis on **IM1** – **IM7** and **CIM2** at 25°C and on samples preheated to 145 °C or 150 °C, past the desolvation point and just below the melt temperature, confirmed a structural change (Fig. S14† and Fig. S15†) and conversion to **NS1** post desolvation (Fig. 9). PXRD analysis on **NS2** at 25°C and at 150 °C, past the main melt and just below the second smaller melt peak, also confirmed a structural change (Fig. S16 †) and conversion to **NS1** (Fig. 9). PXRD analysis of **IM1** – **IM7**, **CIM2**, **NS1** and **NS2**, preheated to 184 °C beyond the recrystallisation point, confirmed conversion to the same unidentified (**UN1**) product (Fig. 10). PXRD analysis of **CIM1** at 25°C and on samples preheated to 145 °C (Fig. 9), past the desolvation point just below the melt temperature, confirmed a structural change (Fig. S16 †) and that desolvation did not lead to **NS1** (Fig. 9) but to an unidentified product (**UN2**). PXRD analysis of **UN2**, preheated further to 189 °C, confirmed a further structural change and indicated the formation of a different unidentified recrystallisation product **(UN3)** to that of **UN1**.

IM desolvation to NS1 and its thermal stability

The desolvation of **IM1** – **IM7** and **CIM2** does not lead to a porous structure with accessible void space, instead there is conversion to **NS1**, meaning the IMs have virtual porosity only (Fig. 11). This lack of stability of an empty host framework is unsurprising as guest removal leads to an unsatisfied hydrogen bonding group (5-nitroisophthalic acid hydroxyl) which must be fulfilled according to Etter's rules. [25] The conversion to **NS1** results in the fulfilment of the hydrogen bonding capabilities of this group, accompanied by the replacement of the solvent in the hydrogen bonded ring host network with an *N*-phenylurea molecular building block.

In the case of **IM7**, the fact an empty host network is not formed is more surprising; guest removal can occur from the channels without disrupting the hydrogen bonded ring. This suggests that the formation of **NS1** is highly favourable. On desolvation of **IM1** – **IM7**, and **CIM2**, to **NS1** a layered structure is also retained which, in the case of **IM2**, becomes increasingly flat. On desolvation of **IM1** – **IM7**, and **CIM2**, to **NS1**, *N*-phenylurea remains the major component where the ratio of molecular building blocks changes from 3:2 in the IMs (7:4 in the case of **IM1**) to 2:1 in **NS1**, for the *N*-phenylurea and 5-nitroisophthalic acid molecular building blocks, respectively. In contrast, upon desolvation of **CIM2** to **NS1**, the ratio of molecular building blocks changes from 1:1, where the host components are present in equal amounts, to 2:1, where *N*-phenylurea is the major component. The structural changes on desolvation are most significant for **IM6**, where the expanded hydrogen bond network condenses, for **IM7**, which switches a carboxylic acid dimer $R_2^2(8)$ hydrogen bond synthon for a carboxylic acid:amide $R_2^2(8)$ hydrogen bond synthon, and for **CIM2**, which adopts a more planar structure and a significant molecular rearrangement occurs. The desolvation to **NS1** leads to a reduction in cell volume and retention of triclinic symmetry in the majority of cases; exceptions to this are **IM7**, where desolvation instead leads to a marginal Increase in cell

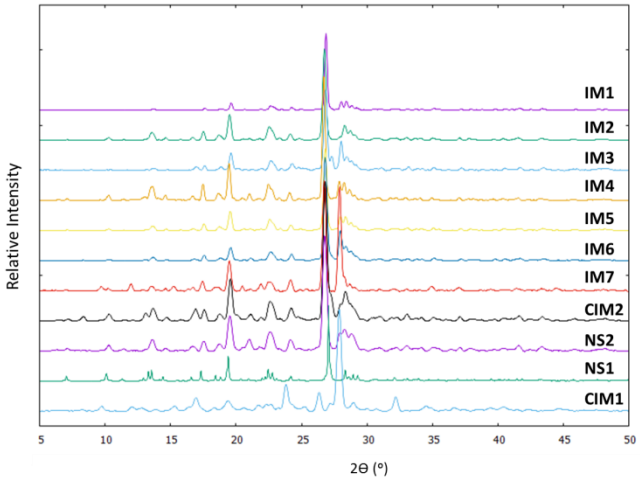

Fig. 9 PXRD patterns of **IM1** – **IM7**, **CIM1**, **CIM2** and **NS2** preheated to 145 or 150 °C compared to that of **NS1**.

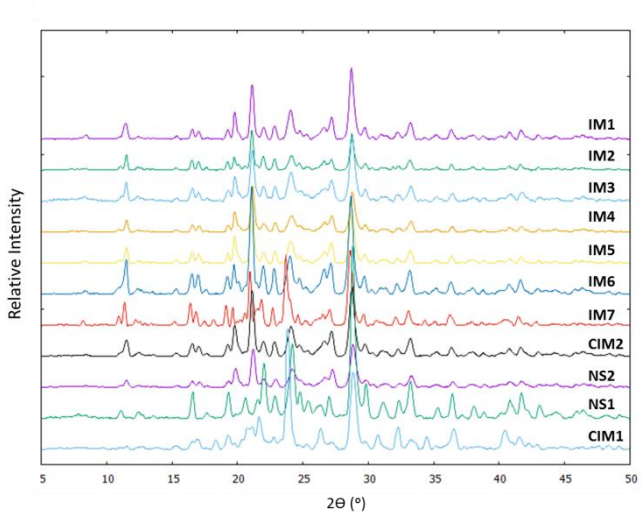

Fig. 10 PXRD patterns of the resulting products after heating **IM1** – **IM7**, **CIM1**, **CIM2**, **NS1** and **NS2** past the recrystallisation point, to 184 °C (189 °C for **CIM1**).

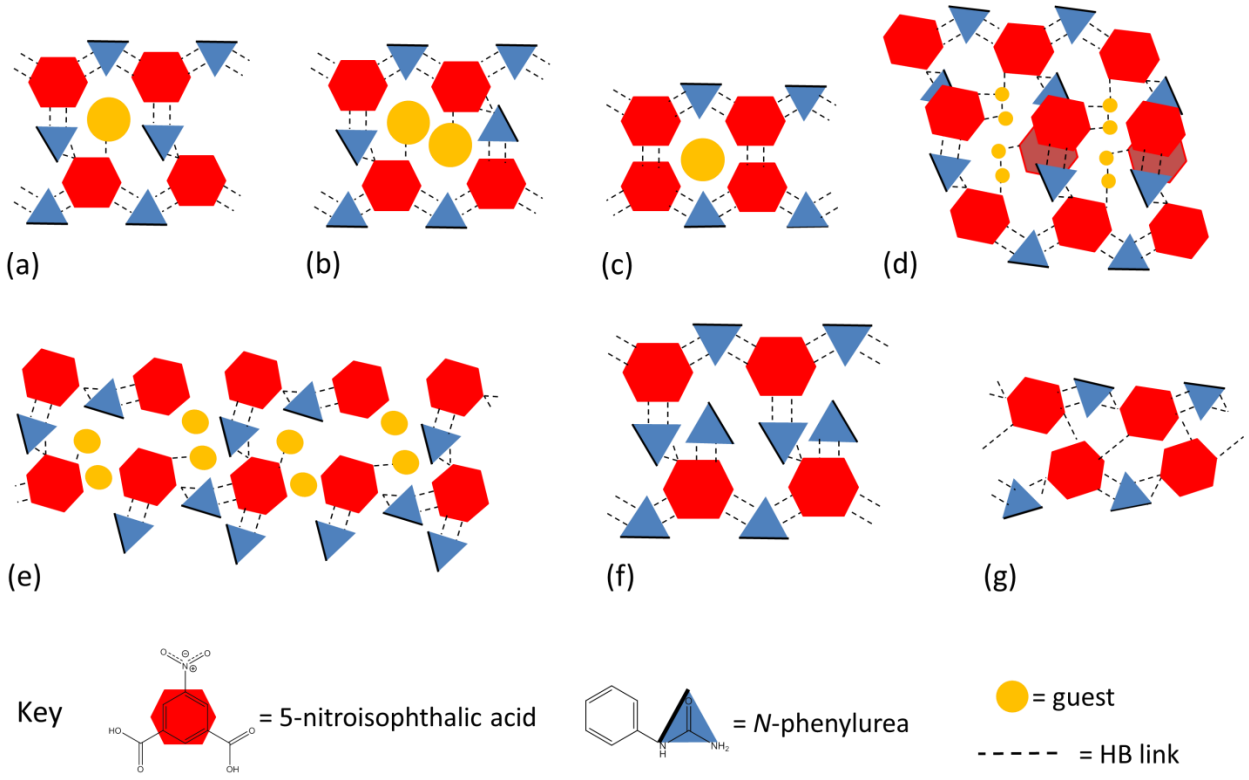

Fig. 11 The arrangement of molecular building blocks in (a) **IM1** – **IM5**, (b) **IM6**, (c) **IM7**, (d) **CIM1**, (e) **CIM2**, (f) **NS1**, (g) **NS2**.

volume, and **CIM2**, where desolvation occurs alongside a change in symmetry from monoclinic to triclinic. The desolvation of **IM1** – **IM6**, and **CIM2**, to **NS1** also leads to an increase in crystal density (Table 10) and a change in the interlayer spacing (Table 11); the largest change is observed in **IM4** and **IM5**. This is not case for **IM7**, crystal density is instead reduced on converting to **NS1**.

The selective conversion of **IM1** – **IM7** and **CIM2** to **NS1**, on desolvation, rather than to **NS2** (which is only produced here by crystallisation from diethyl ether) may be related to several factors including thermal stability, stoichiometries and the nature of the hydrogen bond network. **NS1** has a greater thermal stability than **NS2**, shown by conversion of **NS2** on heating to **NS1**, and is therefore likely to be the thermodynamically more favourable desolvation product; the main melt for **NS2** occurs at T_{onset} 134.7 °C compared with T_{onset} 163.0 °C for **NS1**. The ratio of host molecular building blocks, where *N*-phenylurea is in the majority, is also retained in **NS1** whereas in **NS2**, *N*-phenylurea and 5-nitroisophthalic acid components crystallise in an equivalent 2:2 ratio; it may be that the stoichiometries with excess *N*-phenylurea are more favourable. In **CIM2**, the ratio of host molecular building blocks is actually most similar to **NS2** where the *N*-phenylurea and 5-nitroisophthalic acid components are present in equivalent proportions. The selective conversion of **CIM2** to **NS1** may further suggest the favourability of stoichiometries with excess *N*-phenylurea.

Table 10 Crystal density for **IM1** – **IM7**, **CIM1** and **CIM2** and **NS1** and **NS2**.

Complex	Density (M gm^{-3})
IM1	1.462
IM2	1.403
IM3	1.428
IM4	1.424
IM5	1.44
IM6	1.431
IM7	1.517
CIM1	1.505
CIM2	1.407
NS1	1.496
NS2	1.538

Table 11 Interlayer spacing for **IM1** – **IM7**, **CIM1** and **CIM2** and **NS1** and **NS2**.

Complex	Interlayer spacing (Å)
IM1	3.137(3) – 3.405(3)

IM2	3.008 (9) – 3.389(9)
IM3	2.916(2) – 3.386(2)
IM4	3.187(8) – 3.680(1)
IM5	3.027(2) –3.697(2)
IM6	3.046(3) – 3.359(3)
IM7	3.182(3) – 3.397(4)
CIM1	3.093(5) – 3.332(5)
CIM2	2.987(1) – 3.318(1)
NS1	3.190(3) – 3.367(3)
NS2	2.9974(4) – 3.330(4)

The hydrogen bonded ring host network is the most similar between **NS1** and **IM1** – **IM7**, and **CIM2,** where molecular building blocks assemble via more similar hydrogen bonded synthons in contrast to the situation in **NS2**, where only one of the hydrogen bond synthons present in the IMs leads to molecular building block assembly in this structure. **CIM1** does not convert to **NS1** on desolvation, forming **UN2**, and also forms a different recrystallisation product of **UN3**. The fact that **CIM1** does not convert to **NS1** may be related to **CIM1** and **NS1** having similar crystal densities (1.505M gm^{-3} and 1.496M gm^{-3}, respectively) such that conversion would not lead to any favourable gain in crystal density. It could also be that, due to the small size of the guests, the space created on desolvation is too small to allow molecular rearrangement to **NS1**; in the other IMs, where larger solvent molecules are present, rearrangement to **NS1** occurs.

Guest templation of host network formation

Guest molecules appear to exert control on the host structure in the IMs. Changes to the combination of guest species led to alterations in the hydrogen bonded host network formed. For example, in **IM4**, a hydrogen bonded ring network forms in the presence of acetone and water whilst in **CIM1** and **CIM2**, condensed networks form where water or acetone are present singly. In **IM5**, one hydrogen bonded ring network forms in the presence of THF alongside water whilst in **IM7**, the hydrogen bonded ring network is altered in the presence of THF alongside methanol. Changes in the hydrogen bonded host network were also observed on changing the molecular size of the solvent. For example, an expanded hydrogen bonded ring network occurs for the long chain ethyl acetate solvent (in **IM6**) whereas a smaller hydrogen bonded ring network occurs in **IM1** and **IM3** where the solvent molecules are smaller (methanol and acetonitrile, respectively). The second non-solvated form **NS2** is only produced by crystallisation from diethyl ether and it can be proposed that the large volume of the solvent molecules in this case precludes the initial formation of a solvated IM form and instead favours **NS2** formation. The guest may also be exerting control over the host networks related to its polarity and hydrogen bonding ability; inclusion in the majority of cases (except **IM7**) was via a hydrogen bonding interaction to the host. Only IMs with polar guests included were synthesised; although a number of polar and non-polar solvent guests were trialled. **NS2** was formed direct by crystallisation from diethyl ether and the fact that no ring network was formed around a diethyl ether guest may be related to it being non-polar with a hydrogen bond acceptor oxygen atom which is sterically hindered by the diethyl groups. The multiple hydrogen bond donor and acceptor groups of the water guest may have prevented a ring type network forming in **CIM1**; instead a condensed network resulted allowing the hydrogen bond donor acceptor groups of the water molecules to be satisfied. Water was also only included as a guest when crystallised from ethyl acetate from a 1:1 stoichiometric ratio of the *N*-phenylurea and 5-nitroisophthalic acid host components whilst crystallisation from water from a 2:1 stoichiometric ratio of components presented a direct route to **NS1**. Attempts were made to alter the hydrogen bonding network via changing the set up ratio of components, however in all cases (except in the formation of **CIM1** occurring from a different solvent to that included) this had no effect on the network formed. This further suggests the templating role of guest molecules in these materials.

Unidentified conversion products

The presence of a more stable higher temperature form of **NS1** (**UN1**) is suggested by both DSC and PXRD analysis however the identity of this product is unknown. Unlike **IM1** – **IM7** and **CIM2**, **CIM1** does not convert to **NS1**; instead different unidentified desolvation (**UN2**) and recrystallisation (**UN3**) products are formed. Preliminary indexing and Pawley fits were carried out on the powder patterns of **UN1**, **UN2** and **UN3** in TOPAS v5 [38] to obtain unit cell parameters for these materials. The indexing was inconclusive and further investigation is required to identify these materials.

Resolvation studies

Vapour diffusion studies were carried out on powdered samples of **NS1** and **NS2** to attempt their resolvation (Fig. S17 †). Changes in the powder patterns of **NS1** and **NS2** were only indicated after 24 h of vapour diffusion in acetone solvent (at -18 °C) however it was not

possible to confirm the nature of the structural change (Fig. S18 to S19 †).

Conclusions

We have carried out a systematic study on network materials of *N*-phenylurea and 5-nitroisophthalic acid, assembled in different ratios, and their interaction with a selection of polar solvents. In all, eleven structurally similar materials based on their hydrogen bonded networks have been engineered where nine have interesting solvent inclusion properties. In these materials the carboxylic acid:amide $R_2^2(8)$ hydrogen bonding motif was shown to be particularly robust for network formation and the hydrogen bond has shown its importance as an inclusion material design tool. Thermal analysis of all materials suggested that the inclusion materials were not thermally stable but desolvated on heating and for all, except **CIM1**, converted to **NS1**. **CIM1** converted instead to an unknown product, **UN2**. **NS2** was also shown to be less thermally stable than **NS1** converting to this form on heating. **NS1** was shown to convert to an unknown higher temperature phase **UN1**. These materials therefore do not offer the potential for porous frameworks on guest removal but may yet have applications in exchange or selectivity studies related to the way the guest is held in the host network. In these materials, the guest has been shown to have an important role in determining host structure having a 'templating' effect; different host networks were formed for different combinations of single and multiple guests. The templating of host structures by guest molecules is useful in the design of inclusion materials, allowing the introduction of diversity into the networks and providing the potential for making subtle modifications to structure and therefore properties. The inclusion of different guests in different networks, or not, may also indicate the determining factors in guest selection; here molecular size and hydrogen bond donor acceptor ability appeared to be important.

Acknowledgements

We would like to thank the Chemical Characterisation and Analysis Facility (CCAF) at the University of Bath (www.bath.ac.uk/ccaf) for the provision of the Materials characterisation (TG-MS) facilities.

We acknowledge the support from University of Bath and the Diamond Light Source Ltd for a studentship to L.K.S. CCW and PRR are grateful to the EPSRC for continued support (EP/K004956/1). We would also like to thank the ALS, LBNL for beamtime to collect on **IM2** and S. J. Teat and K. J. Gagnon for assistance. The Advanced Light Source is supported by the Director, Office of Science, Office of Basic Energy Sciences, of the U.S. Department of Energy under contract no. DE-AC02-05CH11231.

Notes and references

1. G. R. Desiraju, *Crystal Engineering: The Design of Organic Solids*, Elsevier, 1989.
2. O. Danylyuk, H. Butkiewicz, A. W. Coleman and K. Suwinska, *CrystEngComm*, 2015, **17**, 1745-1749.
3. K. Buhlmann, J. Reinbold, K. Cammann, K. Skobridis, A. Wierig and E. Weber, *Fresenius J. Anal. Chem.*, 1994, **348**, 549-552.
4. A. Goldup and G. W. Smith, *Sep. Sci. Technol.*, 1971, **6**, 791-817.
5. E. Barea, C. Montoro and J. A. Navarro, *Chem. Soc. Rev.*, 2014, **43**, 5419-5430.
6. O. Korb and P. A. Wood, *Chem. Commun.*, 2010, **46**, 3318-3320.
7. S. G. Frank, *J. Pharm. Sci.*, 1975, **64**, 1585-1604.
8. K. D. M. Harris and J. M. Thomas, *J. Chem. Soc., Faraday Trans.*, 1990, **86**, 2985-2996.
9. S. H. Dale, M. R. J. Elsegood and A. E. L. Coombs, *CrystEngComm*, 2004, **6**, 328.
10. M. Fogagnolo, G. Fantin and O. Bortolini, *Int. J. Mol. Sci.*, 2007, **8**, 662-669.
11. L. J. Barbour, *Chem. Commun.*, 2006, 1163-1168.
12. M. A. Little, M. E. Briggs, J. T. Jones, M. Schmidtmann, T. Hasell, S. Y. Chong, K. E. Jelfs, L. Chen and A. I. Cooper, *Nat. Chem.*, 2014, **7**, 153-159.
13. C.-K. Lam and T. C. W. Mak, *Cryst. Eng.*, 2000, **3**, 33-40.
14. Q. Li and T. C. W. Mak, *Acta Crystallogr., Sect. B: Struct. Sci., Cryst. Eng. Mater.*, 1996, **52**, 989-998.
15. M. J. Horner, S. Grabowski, K. Sandstrom, K. T. Holman, M. Bader and M. C. Ward, *ACA Trans.*, 2004, **39**, 1-10.
16. M. J. Horner, K. T. Holman and M. D. Ward, *J. Am. Chem. Soc.*, 2007, **129**, 14640-14660.
17. M. Etter, D. Parker, S. Ruberu, T. Panunto and D. Britton, *J. Inclusion Phenom. Mol. Recognit. Chem.*, 1990, **8**, 395-407.
18. S. Bhattacharya and B. K. Saha, *Cryst. Growth Des.*, 2011, **11**, 2194-2204.
19. M. C. Etter and G. M. Frankenbach, *Chem. Mater.*, 1989, **1**, 10-12.
20. M. C. Etter, J. C. MacDonald and J. Bernstein, *Acta Crystallogr. Sect. B: Struct. Sci., Cryst. Eng. Mater.*, 1990, **46**, 256-262.
21. O. Ermer and J. Neudörfl, *Helv. Chim. Acta*, 2001, **84**, 1268-1313.
22. A. Alhalaweh, S. George, D. Boström and S. P. Velaga, *Cryst. Growth Des.*, 2010, **10**, 4847-4855.
23. R. Custelcean, *Chem. Commun.*, 2008, 295-307.

24. A. O. F. Jones, C. K. Leech, G. J. McIntyre, C. C. Wilson and L. H. Thomas, *CrystEngComm*, 2014, **16**, 8177-8184.
25. M. C. Etter, *Acc. Chem. Res.*, 1990, **23**, 120-126.
26. Agilent, *CrysAlis Pro Agilient Technologies Ltd., Yarnton, Oxfordshire, England*, 2014.
27. Bruker, *APEX2, Bruker AXS Inc., Madison, Wisconsin, USA*, 2012.
28. Bruker, *SADABS, Bruker AXS Inc., Madison, Wisconsin, USA*, 2001.
29. G. Sheldrick, *Acta Crystallogr. Sect. A: Found. Adv.*, 2008, **64**, 112-122.
30. P. Muller, R. Herbst-Irmer, A. L. Spek, T. R. Schneider and M. R. Sawaya, *Crystal Structure Refinement: A Crystallographer's Guide to SHELXL*, Oxford University Press, Oxford, 2006.
31. L. Farrugia, *J. Appl. Crystallogr.*, 2012, **45**, 849-854.
32. R. C. Bott, G. Smith, U. D. Wermuth and N. C. Dwyer, *Aust. J. Chem.*, 2000, **53**, 767-777.
33. S. V. Kolotuchin, E. E. Fenlon, S. R. Wilson, C. J. Loweth and S. C. Zimmerman, *Angew. Chem., Int. Ed.*, 1996, **34**, 2654-2657.
34. H. I. Süss and J. Hulliger, *Microporous Mesoporous Mater.*, 2005, **78**, 23-27.
35. E. Haldoupis, S. Nair and D. S. Sholl, *Phys. Chem. Chem. Phys.*, 2011, **13**, 5053-5060.
36. C. F. Macrae, P. R. Edgington, P. McCabe, E. Pidcock, G. P. Shields, R. Taylor, M. Towler and J. van de Streek, *J. Appl. Crystallogr.*, 2006, **39**, 453-457.
37. H. Wahl, D. A. Haynes and T. le Roex, *CrystEngComm*, 2015, **17**, 1549-1555.
38. A. A. Coelho, *TOPAS-Academic: general profile and structure analysis software for powder diffraction data. Version 5. Brisbane, Australia*, 2013.